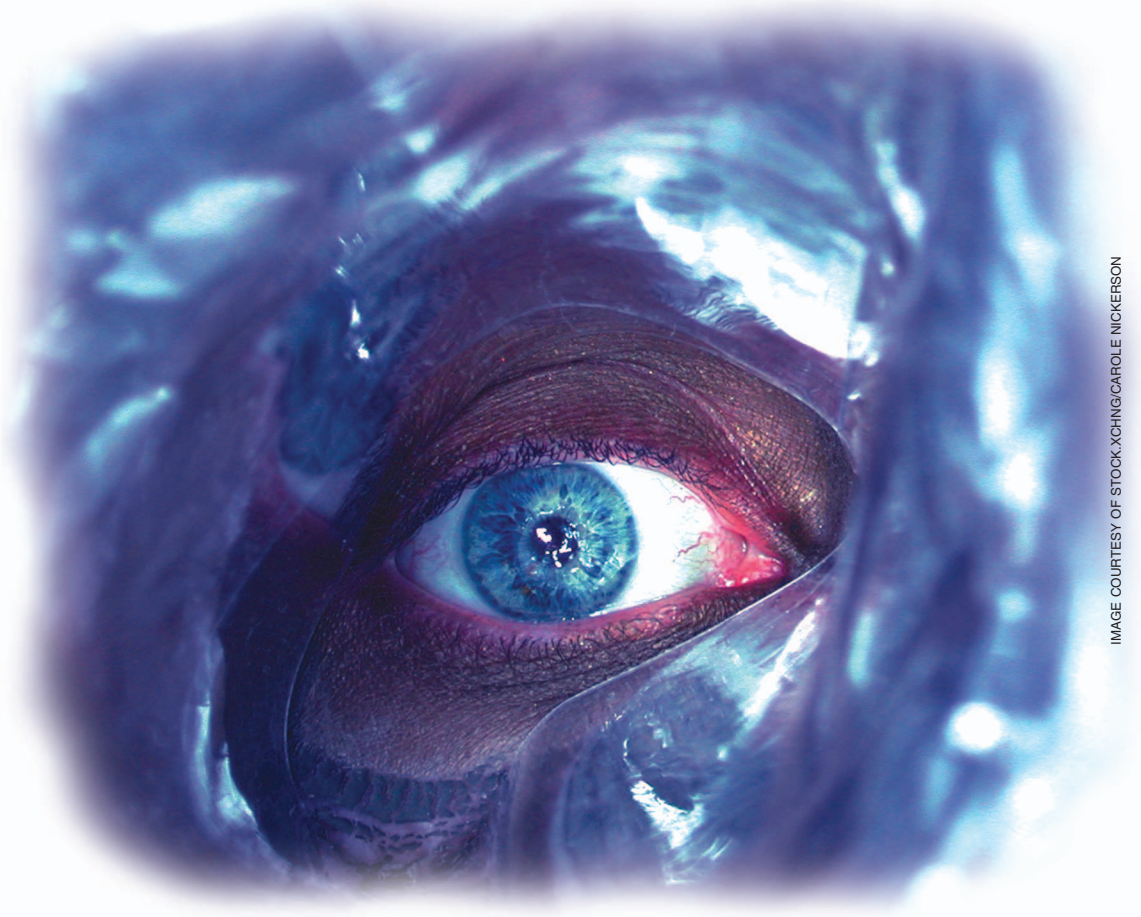

IMAGE COURTESY OF STOCK.XCHNG/CAROLE NICKERSON

Feeling the Pressure

A parylene-based intraocular pressure sensor.

INTRAOCULAR PRESSURE (IOP) is important for the prevention and treatment of certain human eye diseases. For example, glaucoma is the second leading cause of blindness in the world according to the World Health Organization [1]. The majority of glaucoma patients have an IOP $>$ 20 mmHg (compared with a normal IOP of $\sim$10 mmHg), which could damage patients' optic nerves in the backside of the eye and cause irreversible blindness. Currently, there is no cure for glaucoma, but with early diagnosis and proper treatment, the visual loss can be slowed or eliminated. Due to the lack of other symptoms or pain, and the eye's ability to compensate for loss of peripheral vision, many glaucoma patients are unaware of the disease's development until it is severe. In fact, only half of the patients in the United States are aware of having glaucoma. Therefore, early diagnosis and treatment are important to prevent blindness. Thus, a device to diagnose early-stage glaucoma is in demand.

As IOP is a convenient biomarker of glaucoma, clinics generally measure an individual's IOP to determine the presence of the disease. Current clinical IOP measurement is typically done with applanation tonometry. There are primarily two types of applanation tonometers, and both are nonimplantable. The first type of applanation tonometers uses a physical-contact approach to touch the

JEFFREY CHUN-HUI LIN, YU ZHAO, PO-JUI CHEN, MARK HUMAYUN, AND YU-CHONG TAI

Digital Object Identifier 10.1109/MNANO.2012.2203876
Date of publication: 21 August 2012

1932-4510/12/$31.00©2012IEEE

cornea, and the area of the flattened portion is determined by an ophthalmologist. The IOP can then be calculated by the given applanation force and flattened cornea area [2]. The other type of applanation tonometer, named pneumotonometry, obtains IOP by puffing an air jet onto the eye and measuring the flattened portion of the cornea optically [3]. Due to its noncontact characteristics and more accurate optical measurement, pneumotonometry can provide more accurate IOP information than does the contact approach. However, the cornea's mechanical properties and thickness do vary from person to person, so the assumed cornea properties would always introduce errors. Interestingly, it is also reported that, depending on daily activities, a person's IOP can actually raise to as high as 25 mmHg (i.e., above the glaucoma threshold IOP) while the IOP measured in the clinic actually shows a normal value [4]–[8]. Therefore, monitoring of a patient's IOP should be done continuously, 24 hours/seven days a week. Unfortunately, current applanation tonometers cannot provide this capability, as they are only clinical equipment. Therefore, an implant sensor that can monitor IOP continuously and wirelessly is highly desirable [9].

Either active or passive approaches can be adopted to fulfill the telemetric pressure sensing [9]. Although the active devices are more likely to provide more functions, they tend to consume more power during operation. Therefore, power supply is a big issue. In addition, an active implant may require a significant size, which is of special concern for intraocular placement. However, with the infusion of microelectromechanical systems (MEMS) technologies, miniaturized telemetric pressure sensors have already been developed for physiological pressure sensing applications such as intracranial pressure monitoring by Leung et al. [10]. For IOP measurement, McLaren's IOP sensor had a commercial transducer implanted on the dorsal neck of rabbits and a catheter going to the anterior chambers [11]; Mokwa's IOP sensor was designed to be implanted in the lens of the eye [12]; Leonardi et al. built a thin microfabricated platinum–titanium strain gauge on a soft contact lens that can be worn directly on the cornea [13]; Chow et al. designed a tadpole-shaped IOP sensor that would curve along the rim of the anterior chamber after device implantation [14].

As seen from the above examples, there could be different approaches for active IOP sensing. In any case, one must collectively consider the implant size, placement, and the correspondent surgical procedures since the eye is a small and delicate organ and has limited space inside. Here, passive IOP sensors may have many advantages over the active ones in terms of smaller size, little or no power consumption, and easier surgery. One especially interesting passive IOP approach is to use inductor/capacitor resonant circuit (LC)-tank-based sensors with a pressure-dependent capacitor and/or inductor. This approach has also been studied for decades and is well established [15]–[18]. Different physiological pressure monitoring has been achieved using passive telemetry. For example, DeHennis and Wise have adopted the technique to monitor transcutaneous pressure [19] and Fonseca et al. utilized it for pressure monitoring of abdominal aortic aneurysms (AAAs) [20]. For IOP implants, Collins published the first passive wireless transensor implantable in the anterior chamber in 1967 adopting the LC-tank resonant circuit to measure IOP [21]. Backlund et al. modified Collins' IOP sensor design using a capacitive sensor manufactured by a silicon fusion bonding technique [22]–[24]. The capacitor was connected to a hand-wound coil made of 50-μm gold wire to form an LC-tank resonant circuit, and the entire system was encapsulated with silicone for biocompatibility.

This work presents our effort to develop a telemetric-implantable IOP sensor using an LC-tank resonant circuit. In fact, our group presented a flexible parylene-based IOP sensor in 2010 [25]. The sensor had one inductor and one capacitor combined in series as a passive LC-tank resonance circuit. The IOP sensor was implanted into the anterior chamber and anchored on the iris, as shown in Figure 1(a). Figure 1(c) shows the in vivo test of Chen's IOP sensor in a rabbit eye. The resonant frequency shift was registered by an external oscillator circuit through a wireless inductive coupling link. The external interrogating

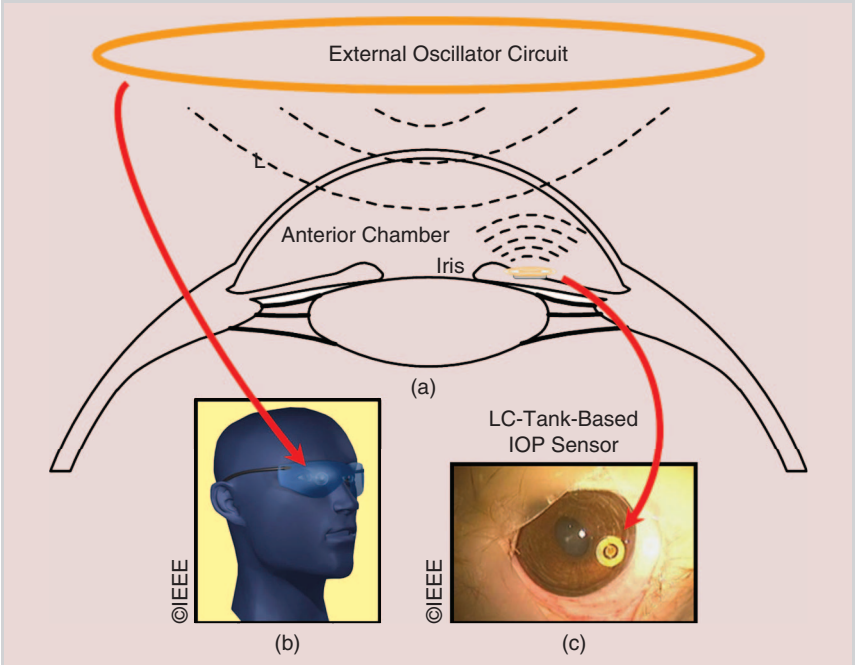

FIGURE 1 (a) Wireless sensing concept of an implantable IOP sensor in the anterior chamber, (b) the glass reader paradigm (published by Chen in 2010 in Fig. 2(a) [25]), and (c) a real IOP sensor in vivo tested in a rabbit eye (published by Chen in 2010 in Fig. 18(b) [25]).

circuit could be designed and integrated into a pair of glasses as shown in Figure 1(b). With the sensor's principle shown in Figure 2(a), when the surrounding pressure increases, the capacitance increases as the sensing plate deforms concavely, introducing resonant frequency shifts to the lower range.

Although the IOP sensor could successfully measure the pressure information of the eye, the anchoring of the sensor was still an issue. In Chen's work, a modified iris retractor was attached to the bottom of the IOP sensor so that the sensor can anchor on top of the iris after implantation. However, the iris would contract or expand frequently and the iris retractor might get loose. In addition, due to the high loss tangent of the eye fluid in the anterior chamber, the LC tank's quality factor was degraded, and the sensing distance is reduced just like other wireless sensors [20], [25], [26].

To overcome these problems, a new IOP sensor structure is developed. We keep the sensing part design similar to our previous device, which is composed of a sensing inductor and a sensing capacitor [Figure 3(a)]. A pressure

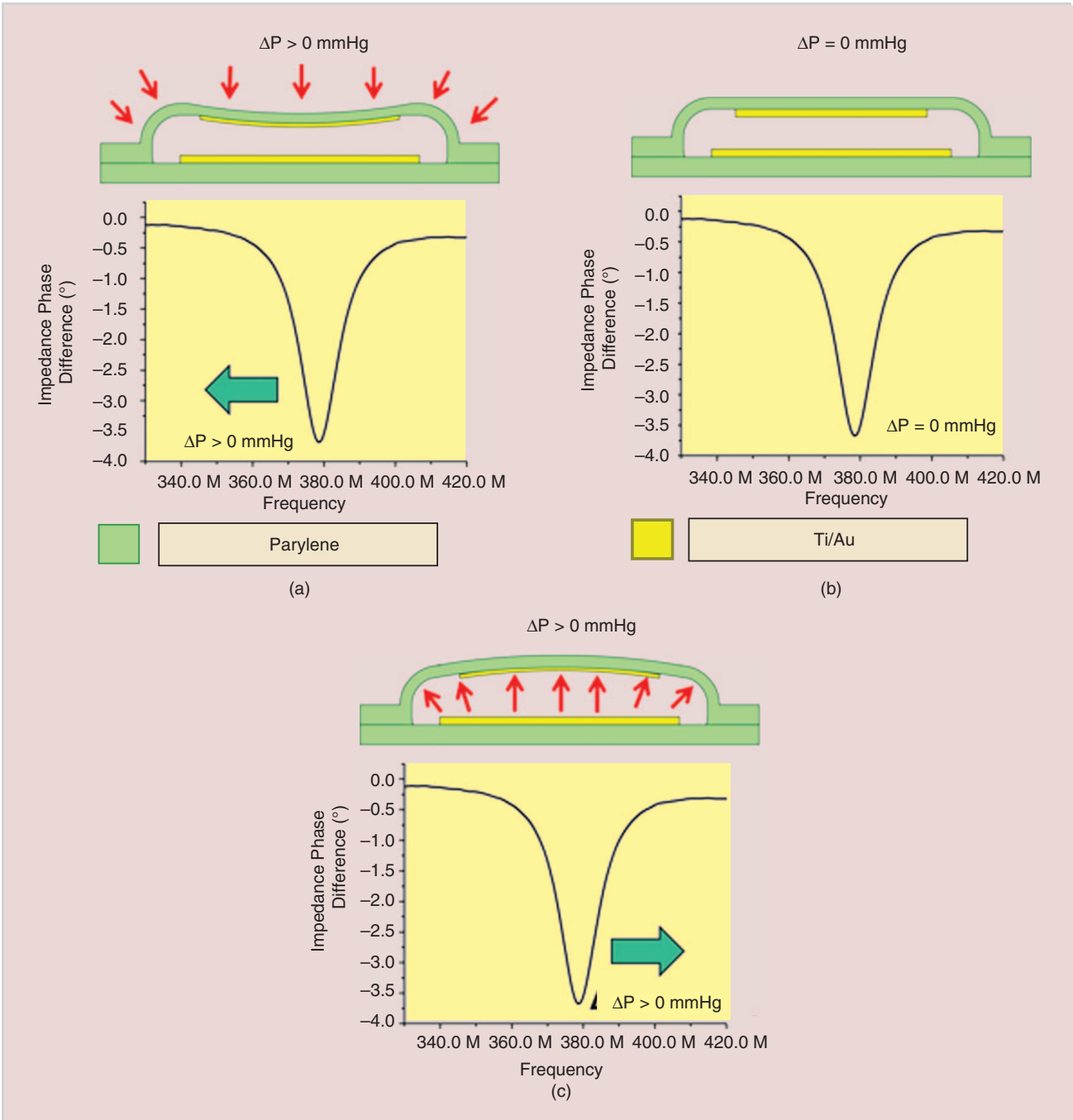

FIGURE 2 Resonant frequency shift corresponds to the applied pressure: (a) frequency decreases as the capacitance increases, (b) no frequency shift observed when no pressure difference exists, and (c) frequency increases as the capacitance decreases.

access hole connecting the chamber of the sensing capacitor and outside is created during device fabrication. The pressure access hole allows an implantation tube to be attached to the backside of the device to cover the access hole as shown in Figure 3(b).During device fabrication, a biocompatible epoxy is applied to seal the gap between the implantation tube and the sensing part to make it airtight and also to ensure the device's biocompatibility.

The newly designed IOP sensor could be placed with an implantation tube penetrating the eyeball choroid through the pars plana while the sensing part remains outside the choroid but under the conjunctiva of the eye, as shown in Figure 4. This kind of placement is similar to that of [27].

In addition, this work also includes a designed passivation to retain the high quality factor of the device. Although the sensing coil is kept outside the eyeball in this new implantation, the tissue under the conjunctiva still imposes power absorption so that the sensor's quality factor is reduced. To counter this, we adopt an approach of parylene-C passivation in which adequate parylene-C is deposited to contain the electric field induced between different coils. By quantitatively measuring the effect of parylene-C passivation with different parylene-C thicknesses, the results show that the quality factor of the sensing coil immersed in saline can indeed be recovered to the original value as in air, and the passivation enables to sense longer distances after implantation. As shown in Figure 5, it is concluded that an extra 20-μm parylene-C passivation layer applied on top of the original sensing coil, on which already has 15-μm parylene-C covered, helps maintain the high quality factor of the sensor when it is covered by human body tissues.

SENSING THEORY AND THE DEVICE DESIGN

SENSING SCHEME

The wireless sensing scheme is shown in Figure 6. The right electrical circuit consisting of a resistor, an inductor, and a capacitor represents the implanted IOP

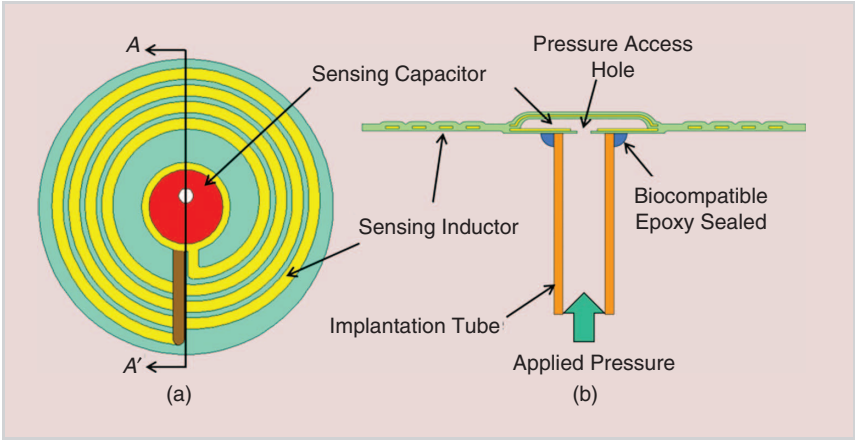

FIGURE 3 The new IOP sensor design: (a) top view of the sensing part and (b) AA′ cross-section view of the IOP sensor.

sensor, and its resonant frequency can be expressed as [26]

$$f_s = \frac{1}{2\pi}\sqrt{\frac{1}{L_s C_s} - \frac{R_s^2}{L_s^2}} \cong \frac{1}{2\pi\sqrt{L_s C_s}} \quad \text{if} \quad R_s^2 \ll \frac{L_s}{C_s}, \quad (1)$$

where R_s, L_s, and C_s represent the resistance, inductance, and capacitance of the sensor, respectively. The equivalent impedance viewed from the external coil reader and apparatus is derived as [18], [20], [28]:

$$z_{\text{eq}} = j2\pi f L_r \left[1 + k^2 \frac{\left(\frac{f}{f_s}\right)^2}{1 - \left(\frac{f}{f_s}\right)^2 + \frac{1}{Q_s} j\frac{f}{f_s}}\right], \quad (2)$$

where f is the excitation frequency and k is the coupling coefficient of the

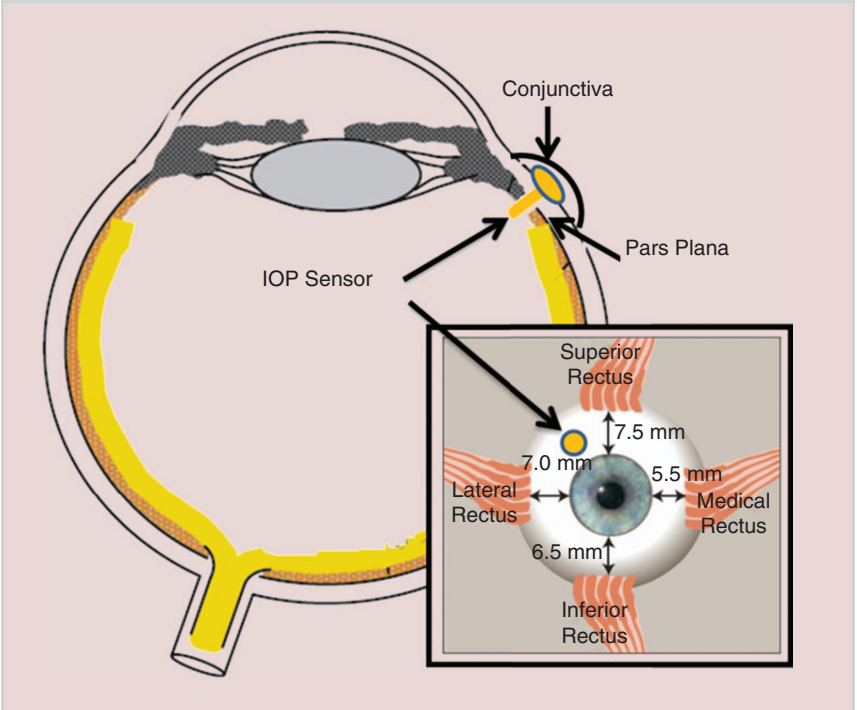

FIGURE 4 The newly designed IOP sensor is implanted at the pars plana with the implantation tube going through the choroid while the sensing part still remains outside the choroid but under the conjunctiva of the eye.

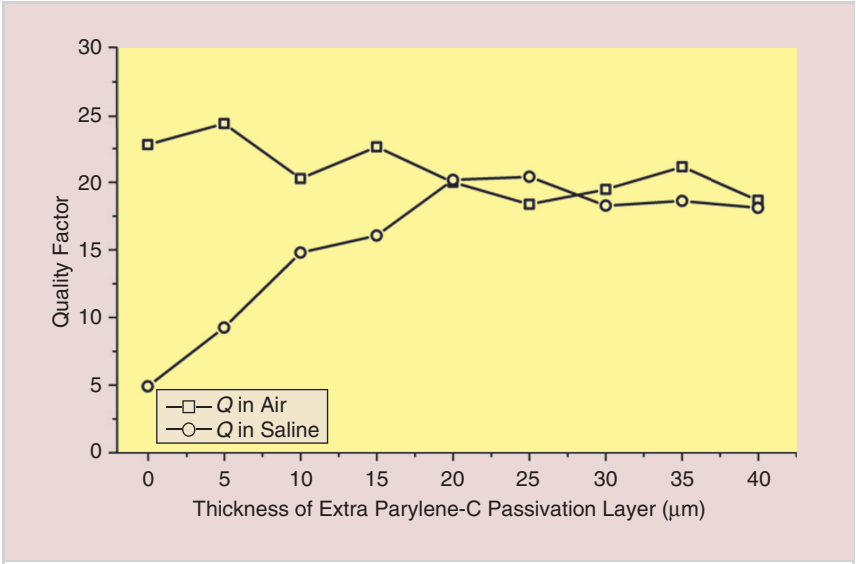

FIGURE 5 Quality-factor versus thickness of an extra parylene-C passivation layer. Recovering is achieved by covering the IOP sensor with several 5-μm thick parylene-C layers. The original parylene-C covered on top of the sensing coil is 15 μm thick.

inductive link depending on the dimensions and separation of the coupled coils [17]–[20], [28]. Q_s, the quality factor of the sensor at the resonance, can be represented as

$$Q_s = \frac{1}{R_s\sqrt{L_s C_s}}. \tag{3}$$

When the sensor is excited at the resonant frequency, Z_{eq}, (2) becomes

$$Z_{\text{eq}} = j2\pi f_s L_r(1 + jk^2 Q_s), \tag{4}$$

and its phase dip magnitude can be approximated as

$$\Delta\phi \cong \tan^{-1}(k^2 Q_s), \tag{5}$$

when the capacitance of the IOP sensor changes, (3)–(5) show that the impedance phase dip shifts to either lower or higher frequency, which can be detected by a network analyzer.

ELECTRICAL AND MECHANICAL DESIGN OF THE DEVICE

The electrical design of the IOP sensor can be explained by the well-developed equations as follows [15], [25], [29]. The inductance of the spinal coil can be represented as

$$L_s \cong \frac{\mu_0 n^2 d_{\text{avg}} c_1}{2}\left[\ln\left(\frac{c_2}{F}\right) + c_3 F + c_4 F^2\right], \tag{6}$$

where n is the number of turns of the inductor, d_{avg} is the averaged diameter of the coil windings, $F = (d_{\text{out}} - d_{\text{in}})/(d_{\text{out}} + d_{\text{in}})$ is the fill factor of the coil windings, and $c_1 - c_4$ are constants determined by the winding geometry. The coil winding inherently comes with a resistance and can be calculated as

$$R_s = \frac{\rho l}{w\delta(1 - e^{-h/\delta})}, \tag{7}$$

where ρ is the electrical resistivity of the metal and w and h are the metal line width and height, respectively. δ is the frequency-dependent metal skin depth that can be written as

$$\delta = \sqrt{\frac{\rho}{\pi f \mu}}, \tag{8}$$

where μ is the magnetic permeability of the metal. The capacitance of the IOP sensor is given by

$$C_s = C_{s,g} + C_{s,p}, \tag{9}$$

where $C_{s,g}$ is the capacitance of the parallel metal plate capacitor at the center of the IOP sensor and $C_{s,p}$ is the parasitic/stray capacitance introduced by other components in the entire device.

To have a detectable impedance phase dip shift, a deformable circular metal plate was designed at the center of the IOP sensor. Once the plate deforms either downward or upward, the capacitance of the parallel-metal-plate capacitor changes and impedance-phase dip shifts can be registered. The deformation of the metal plate corresponding to the pressure difference can be predicted as [30]:

$$w(r) = \frac{\Delta P a^4}{64D}\left[1 - \left(\frac{r}{a}\right)^2\right]^2, \tag{10}$$

where Δp is the pressure difference, r is the radius calculated from the center of the plate, a is the diaphragm radius, and D is the flexural rigidity of the diaphragm.

In our new sensor implantation approach, the sensing metal plate deforms convexly with higher surrounding pressure transmitted to the metal diaphragm capacitor chamber through the implantation tube. According to (1), this higher eye pressure causes the capacitance to reduce and, thus, the resonant frequency shifts to a higher range, as described in Figure 2(c).

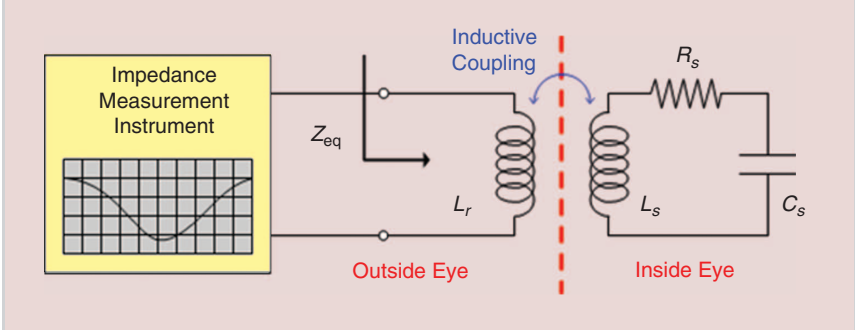

FIGURE 6 The concept of a wireless inductive coupling link. The frequency shift is registered through an external oil reader.

DEVICE FABRICATION AND CHARACTERIZATION

DEVICE FABRICATION

The fabrication procedure of the sensing coil is shown in Figure 7. The sensing part was made of a parylene–gold (3-μm)–parylene sandwich structure. The first layer of 5-μm parylene-C was deposited on top of a layer of sacrificial photoresist. The pressure access hole with 180 μm in diameter was opened by oxygen plasma. A 3-μm Ti/Au was deposited on top of the first-layer parylene-C and patterned. The distance between two capacitor metal plates was designed as 10 μm and was achieved by spin coating and patterning a 10-μm thick sacrificial photoresist. A second layer of parylene-C was deposited to cover and protect the 3-μm Ti/Au, followed by a 0.5-μm Ti/Au deposition. The third parylene-C layer was then deposited, and the configuration of the sensing part was patterned by oxygen plasma. The sensing part was finally released from the substrate by soaking in acetone. The completed sensing part is shown in Figure 8(a).

After completing the fabrication of the sensing part, the implantation tube was attached onto the backside, as shown in Figure 8(b). The inner diameter of the implantation tube was chosen as 320 μm to fully cover the pressure access hole. The outer diameter of the implantation tube was 450 μm. The implantation tube was manually mounted onto the sensing part. A precision XYZ stage was used to control the position of the implantation tube that was maneuvered to be concentric with the pressure access hole. The implantation tube and sensing part were glued together with a few drops of biocompatible epoxy.

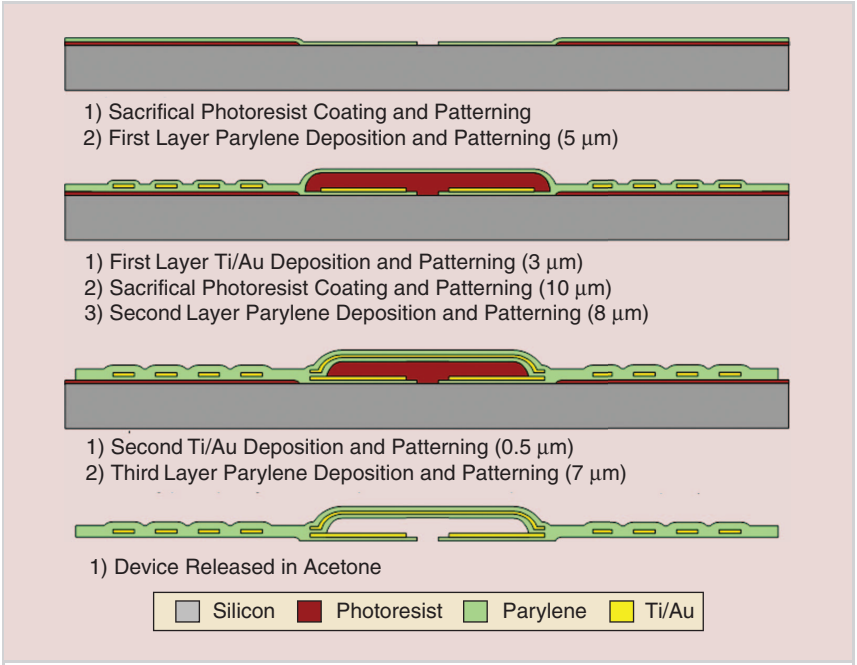

FIGURE 7 Fabrication procedures of the sensing part of the IOP sensor.

DEVICE CHARACTERIZATION

The completed IOP sensor was then integrated to a bigger testing capillary tube and sealed by photoresist, as shown in Figure 8(c). The inner diameter of the testing tube was chosen as 500 μm to accommodate the implantation tube. The completed sensor with testing capillary tube assembly was left overnight to dry the photoresist.

The device characterization setup is shown in Figure 9. The whole IOP sensor assembly was mounted onto a pressure characterization setup. During characterization, an HP 4195A network/spectrum analyzer was hooked up with a 1.5-mm-diameter hand-wound coil serving as the reader coil. The characterization signal was accessed via a data acquisition system and then analyzed in a personal computer. The qualified IOP sensor was released by soaking the whole assembly in acetone to remove the photoresist. The final IOP sensor is shown in Figure 8(d) and is ready for the next in vivo/ex vivo test.

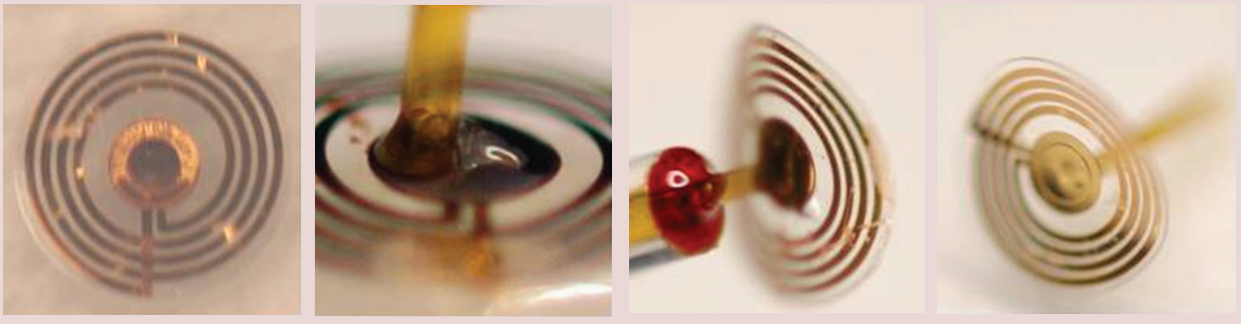

FIGURE 8 IOP sensor fabrication and assembling results: (a) the completed sensing part, (b) an implantation tube attached onto the backside of the sensing part concentric with the pressure access hole, (c) an IOP sensor mounted to the testing tube by photoresist, and (d) the final IOP sensor.

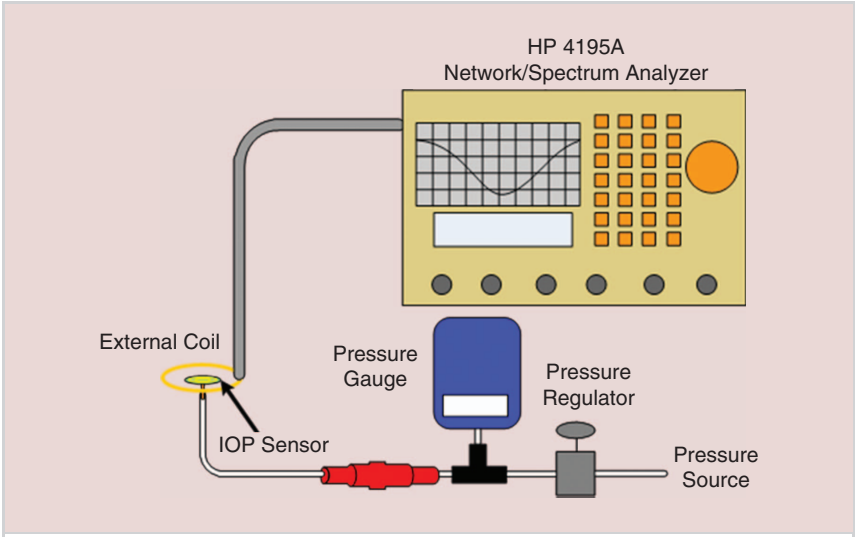

FIGURE 9 IOP sensor characterization setup: a 1.5-mm-diameter hand-wound coil served as the reader coil and an HP 4195A network/spectrum analyzer was used to register the frequency shift of the phase dip.

CHARACTERIZATION RESULTS

The benchtop characterization results are shown in Figure 10. The results show that the resonant frequency was 379 MHz when the applied pressure difference was 0 mmHg. When the applied pressure difference increased, the resonant frequency shifted to the right, as expected, because the metal plate deformed convexly. The IOP sensor's electrical parameters were obtained and shown in Table 1.

As the sensing part can always be maintained exposed outside the anterior chamber, the quality factor drop caused by the lossy medium is largely alleviated in this work. Therefore, the new implant possesses a farther sensing distance than the one implanted right in the anterior chamber, which was originally designed to have a 2.5-cm sensing distance. The new design enables a glass reader paradigm to accomplish autonomous, continuous, and wireless IOP monitoring. The result of sensitivity analysis is shown Figure 11. The sensitivity of the IOP sensor is defined as [26]

$$\left|\frac{\partial R}{\partial(\Delta P)}\right|_{\Delta P=0}, \tag{11}$$

where R is the frequency ratio defined as

$$R = \frac{f_{\min}}{f_{\min\,(\Delta p=0)}}. \tag{12}$$

A sensitivity of 542 ppm/mmHg was obtained for the IOP sensor, corresponding to the responsivity as 205 kHz/mmHg. With a properly designed high-resolution external coil reader, the IOP sensor can resolve the pressure difference < 1 mmHg, which is suitable for glaucoma diagnostics.

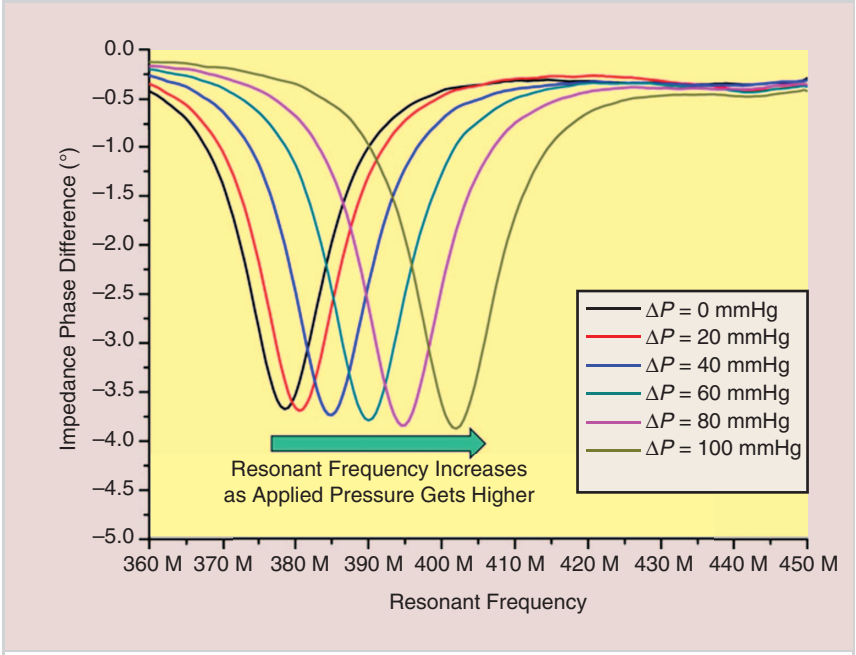

FIGURE 10 Benchtop characterization results of the IOP sensor. The resonant frequency was 379 MHz when the applied pressure difference was 0 mmHg and shifted to a higher frequency when the pressure difference increased.

QUALITY FACTOR RECOVERY STUDY

As mentioned in [25], the quality factor of the transmitting coil, i.e., transmitting resonant tank, dropped significantly when implanted in the anterior chamber, which resulted in a great reduction of sensing distance. As the loss tangent represents the power loss in the medium, this quality factor drop is due to the high loss tangent of the eye fluid in the anterior chamber. The loss tangent value of saline is reported at about 0.2 [20], [31], which is much higher than of the air and close to that of body tissue and eye fluid. This means that the electromagnetic energy of the IOP sensor dissipates more easily in the anterior chamber. Although in our work, only the implantation tube penetrates into the eyeball and leaves the sensing part under the conjunctiva, the quality factor can still drop due to the covering human body tissues.

Therefore, to restore the high quality factor, quantitative investigation has also been done by putting multilayer parylene-C films on top of the sensing coil to regain its quality factor when it is submersed in the saline. The concept of the experiment is shown in Figure 12. An original sensing coil with 15-μm

parylene-C deposited on top was first mounted onto a glass slide. Multiple 5-μm-thick parylene-C films were put layer by layer on top of the sensing coil. Before the next 5-μm parylene-C film was put on, the coil was characterized, both exposed in air, and also submersed in saline. The quality factors were calculated to investigate the quality factor recovery capability with respect to different parylene-C thicknesses.

The sensor's quality factor measuring result versus thickness of an extra parylene-C passivation layer is shown in Figure 5. When only 15-μm thick parylene-C covers the top of the sensing coil (the original sensing coil), it can be seen that the quality factor is measured to be only five in saline while it is measured as 23 in air. The obtained quality factors (in saline) increase with increasing parylene-C thickness and saturates to 17–20 when the thickness of the extra parylene-C passivation layer reaches 20 μm. We conclude that the sensing coil will not be affected by the surrounding saline when the thickness of the overall covering parylene-C layer reaches 35 μm. It is therefore proved that a 35-μm-thick parylene-C passivation layer is sufficiently thick to be deposited on top of the metal coil. It is also found that the quality factor measured with the device exposed in the air drops a bit as the parylene-C passivation layer increases. It is likely due to the low loss tangent of parylene-C.

CONCLUSION

We have successfully demonstrated the feasibility of the new concept and design of the IOP sensor implant. A surgical placement of the device at the pars plana is also proposed. We demonstrated that a 35-μm-thick parylene-C can maintain a high quality factor of sensor in saline or under human tissue. The new IOP sensor can allow continuous and wireless IOP monitoring.

ACKNOWLEDGMENT

This work is supported by the Biomimetic MicroElectronic Systems (BMES) Center under grant no. H31068. The authors thank Trevor Roper for his help with sample preparation, machine maintenance, and instrument installation.

TABLE 1 Dimension of the new IOP sensor and its measured electrical parameters.

Planar Dimension	4 mm (Foldable)					
Pressure (mmHg)	0	20	40	60	80	100
Frequency (MHz)	379	381	385	390	395	402
Q factor	27	27	28	30	28	29
Sensitivity	542 ppm/mmHg					
Responsivity	205 kHz/mmHg					
Sensing distance	2.5 cm					

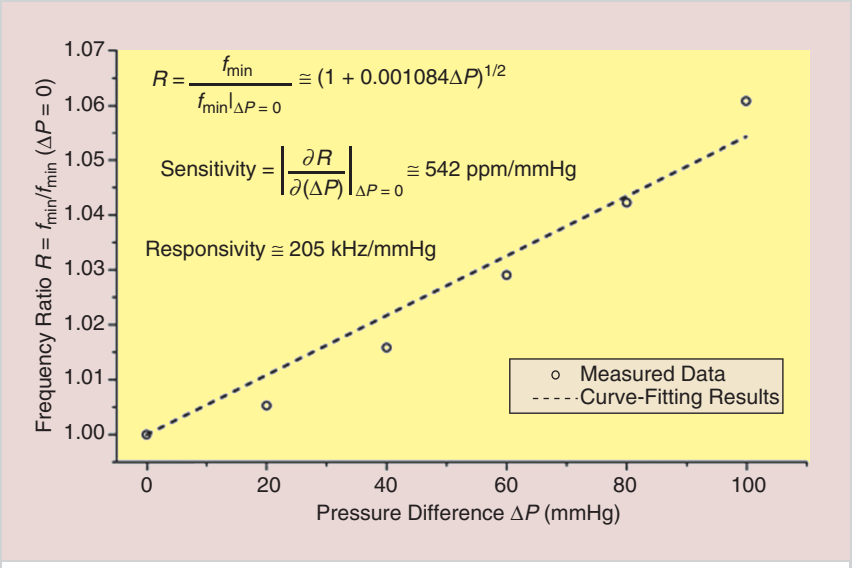

FIGURE 11 Sensitivity analysis of the IOP sensor.

ABOUT THE AUTHORS

Jeffrey Chun-Hui Lin (linch@mems.caltech.edu) received his B.S. degree in mechanical engineering from National Taiwan University, Taipei, in 1999, and his M.S. and Ph.D. degrees in electrical engineering from the California Institute of Technology (Caltech), Pasadena, in 2007 and 2012, respectively. He is currently working at MiniPumps, LLC in Pasadena, California, as a microdevice and quality control engineer.

Yu Zhao (yzhao@mems.caltech.edu) received her B.S. (Hons) degree in electrical engineering from Peking University in 2008 and her M.S. degree from the California Institute of Technology in 2009. She is currently a Ph.D. candidate in Prof. Y.C. Tai's group, focusing on developing wireless power transmission solutions for retinal and spinal cord prosthesis devices.

Po-Jui Chen (pojui.chen@gmail.com) received his B.S. degree in mechanical engineering from National Taiwan University, Taipei, in 2002, and his M.S. and Ph.D. degrees in electrical engineering from the California Institute of

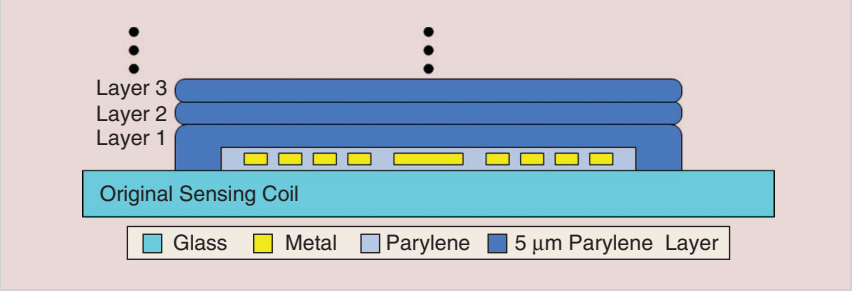

FIGURE 12 Quality factor recovery study by putting multiple layers of parylene-C film on top of the sensing coil.

In our new sensor implantation approach, the sensing metal plate deforms convexly with higher surrounding pressure transmitted to the metal diaphragm capacitor chamber through the implantation tube.

Technology (Caltech), Pasadena, in 2004 and 2008, respectively. He has been active in technology research and development, mainly in the area of MEMS. His research interests include emerging process and manufacture technology, multidisciplinary device/module/system engineering, and technical scouting.

Mark Humayun (MHumayun@doheny.org) received his B.S. degree from Georgetown University, Washington, District of Columbia, in 1984, his M.D. degree from Duke University, Durham, North Carolina, in 1989, and his Ph.D. degree from the University of North Carolina, Chapel Hill, in 1994. He finished his training by completing an ophthalmology residency at Duke University and a fellowship in vitreoretinal diseases at Johns Hopkins Hospital. He is currently a professor of ophthalmology, biomedical engineering, and cell and neurobiology at the University of Southern California, Los Angeles, where he is the director of the National Science Foundation Biomimetic MicroElectronic Systems Engineering Research Center. He is also the director of the Department of Energy Artificial Retina Project that is a consortium of five Department of Energy laboratories and four universities, as well as industry. He is a member of the National Academies of Engineering and the National Academies Institute of Medicine.

Yu-Chong Tai (yctai@its.caltech.edu) received his B.S. degree from National Taiwan University and his M.S. and Ph.D. degrees in electrical engineering from the University of California, Berkeley, in 1986 and 1989, respectively. He developed the first electrically spun polysilicon micromotor at the University of California, Berkeley. He is currently a professor of electrical engineering, mechanical engineering, and bioengineering at the California Institute of Technology (Caltech), Pasadena. He has published more than 300 technical articles in the field of MEMS. He is the recipient of the IBM Fellowship, the Ross Tucker Award, the Best Thesis Award (at Berkeley), the Presidential Young Investigator Award, the Packard Award, and the ALA Achievement Award. His main research interest at Caltech is MEMS for biomedical applications, including lab-on-a-chip and neural implants.

REFERENCES

[1] Glaucoma Research Foundation (2012).[Online]. Available: http://www.glaucoma.org/

[2] Glaucoma. [Online]. Available: http://www.lea-test.fi/en/eyes/glaucoma.html

[3] H. Cao, "Pressure sensors," in *Minimally Invasive Medical Technology*, New York: Taylor & Francis, 2001, pp. 33–45.

[4] E. Hughes, P. Spry, and J. Diamond, "24-hour monitoring of intraocular pressure in glaucoma management: A retrospective review," *J. Glaucoma*, vol. 12, pp. 232–236, June 2003.

[5] R. Sampaole, N. Calixto, C. Decarval, and R. Reca, "Diurnal variation of intraocular pressure in healthy suspected and glaucomatous eyes," *Biblio. Ophthalmol.*, p. 1, 1968.

[6] M. L. Dietsche, J. T. Wilensky, D. K. Gieser, M. T. Mori, and R. Zeimer, "The individual nature of diurnal-variations in intraocular-pressure," *Invest. Ophthalmol. Vis. Sci.*, vol. 32, pp. 809–809, Mar. 1991.

[7] J. T. Wilensky, "Diurnal variations in intraocular pressure," *Trans. Amer. Ophthalmol. Soc.*, vol. 89, pp. 757–790, 1991.

[8] S. Asrani, R. Zeimer, J. Wilensky, D. Gieser, S. Vitale, and K. Lindenmuth, "Large diurnal fluctuations in intraocular pressure are an independent risk factor in patients with glaucoma," *J. Glaucoma*, vol. 9, pp. 134–142, Apr. 2000.

[9] K. C. Katuri, S. Asrani, and M. K. Ramasubramanian, "Intraocular pressure monitoring sensors," *IEEE Sensors J.*, vol. 8, pp. 12–19, Jan.–Feb. 2008.

[10] A. M. Leung, W. H. Ko, T. M. Spear, and J. A. Bettice, "Intracranial-pressure telemetry system using semicustom integrated-circuits," *IEEE Trans. Biomed. Eng.*, vol. 33, pp. 386–395, Apr. 1986.

[11] J. W. McLaren, R. F. Brubaker, and J. S. Fitz-Simon, "Continuous measurement of intraocular pressure in rabbits by telemetry," *Invest. Ophthalmol. Vis. Sci.*, vol. 37, pp. 966–975, May 1996.

[12] W. Mokwa and U. Schnakenberg, "Microtransponder systems for medical applications," *IEEE Trans. Instrum. Meas.*, vol. 50, pp. 1551–1555, Dec. 2001.

[13] M. Leonardi, P. Leuenberger, D. Bertrand, A. Bertsch, and P. Renaud, "First steps toward noninvasive intraocular pressure monitoring with a sensing contact lens," *Invest. Ophthalmol. Vis. Sci.*, vol. 45, pp. 3113–3117, Sept. 2004.

[14] E. Y. Chow, A. L. Chlebowski, and P. P. Irazoqui, "A miniature-implantable RF-wireless active glaucoma intraocular pressure monitor," *IEEE Trans. Biomed. Circuits Syst.*, vol. 4, pp. 340–349, Dec. 2010.

[15] O. Akar, T. Akin, and K. Najafi, "A wireless batch sealed absolute capacitive pressure sensor," *Sensors Actuators A, Phys.*, vol. 95, pp. 29–38, Dec. 2001.

[16] Sajeeda and T. J. Kaiser, "Passive telemetric readout system," *IEEE Sensors J.*, vol. 6, pp. 1340–1345, Oct. 2006.

[17] A. Baldi, W. Choi, and B. Ziaie, "A self-resonant frequency-modulated micromachined passive pressure transensor," *IEEE Sensors J.*, vol. 3, pp. 728–733, Dec. 2003.

[18] M. A. Fonseca, J. M. English, M. von Arx, and M. G. Allen, "Wireless micromachined ceramic pressure sensor for high-temperature applications," *J. Microelectromech. Syst.*, vol. 11, pp. 337–343, Aug. 2002.

[19] A. DeHennis and K. D. Wise, "A double-sided single-chip wireless pressure sensor," *15th IEEE Int. Conf. Micro Electro Mechanical Systems, Tech. Dig.*, 2002, pp. 252–255.

[20] M. A. Fonseca, M. G. Allen, J. Kroh, and J. White, "Flexible wireless passive pressure sensors for biomedical applications," in *Tech. Dig., 12th Solid-State Sensors, Actuators, and Microsystems Workshop*, Hilton Head Island, SC, 2006, pp. 37–42.

[21] C. C. Collins, "Miniature passive pressure transensor for implanting in eye," *IEEE Trans. Biomed. Eng.*, vol. BM14, p. 74, 1967.

[22] Y. Backlund, L. Rosengren, B. Hok, and B. Svedbergh, "Passive silicon transensor intended for biomedical, remote pressure monitoring," *Sensors Actuators A Phys.*, vol. 21, pp. 58–61, Feb. 1990.

[23] L. Rosengren, Y. Backlund, T. Sjostrom, B. Hok, and B. Svedbergh, "A system for wireless intra-ocular pressure measurements using a silicon micromachined sensor," *J. Micromech. Microeng.*, vol. 2, p. 202, 1992.

[24] L. Rosengren, P. Rangsten, Y. Backlund, B. Hok, B. Svedbergh, and G. Selen, "A system for passive implantable pressure sensors," *Sensors Actuators A Phys.*, vol. 43, pp. 55–58, May 1994.

[25] P. J. Chen, S. Saati, R. Varma, M. S. Humayun, and Y. C. Tai, "Wireless intraocular pressure sensing using microfabricated minimally invasive flexible-coiled LC sensor implant," *J. Microelectromech. Syst.*, vol. 19, pp. 721–734, Aug. 2010.

[26] P.-J. Chen, "Implantable wireless intraocular pressure sensors," Ph.D. dissertation, *Elect. Eng.*, California Inst. Technology, Pasadena, CA, 2008.

[27] Ahmed Glaucoma Valve (2012). [Online]. Available: http://www.ahmedvalve.com/

[28] J. Shih, J. Xie, and Y. C. Tai, "Surface micromachined and integrated capacitive sensors for microfluidic applications," *Boston Transducers'03: Dig. Tech. Papers*, vols. 1 and 2, 2003, pp. 388–391.

[29] T. H. Lee, *The Design of CMOS Radio-Frequency Integrated Circuits*, 2nd ed. Cambridge, U.K.: Cambridge Univ. Press, 2004.

[30] S. Timoshenko and S. Woinowsky-Krieger, *Theory of Plates and Shells*, 2nd ed. New York: McGraw-Hill, 1959.

[31] J. M. Kim, D. H. Oh, J. H. Park, J. W. Cho, Y. W. Kwon, C. Y. Cheon, and Y. K. Kim, "Permittivity measurements up to 30 GHz using micromachined probe," *J. Micromech. Microeng.*, vol. 15, pp. 543–550, Mar. 2005.

N